Role of Sterol Superlattice in Free Radical-Induced Sterol Oxidation in Lipid Membranes†

Michelle Olsher, Su-In Yoon, and Parkson Lee-Gau Chong*

Department of Biochemistry, Temple University School of Medicine, Philadelphia, Pennsylvania 19140

Received October 27, 2004; Revised Manuscript Received November 25, 2004

ABSTRACT: We developed a new fluorescence assay for sterol oxidation and used it to study the relationship between free radical-induced sterol oxidation and membrane sterol lateral organization. This assay used dehydroergosterol (DHE) as both a membrane probe and a membrane component. Sterol oxidation was induced by a free radical generator, AAPH (2,2′-azobis(2-amidinopropane)dihydrochloride). Using this new assay, we found that, in unilamellar vesicles composed of DHE and 1-palmitoyl-2-oleoyl-L-α-phosphatidylcholine (POPC), the initial rate of DHE oxidation induced by AAPH changed with membrane sterol content in an alternating manner, exhibiting a local maximum at 20.3, 22.2, 25.0, 32.3, and 40.0 mol % DHE. These mole fractions correspond to the critical sterol mole fractions C_r predicted for maximal sterol superlattice formation. In three-component bilayers composed of POPC, cholesterol, and DHE (fixed at 1 and 5 mol %), the initial rate of AAPH-induced DHE oxidation exhibited a biphasic change whenever the total sterol mole fraction, irrespective of the DHE content, was near C_r, indicating that the correlation between sterol oxidation and sterol superlattice formation revealed in this study is not an artifact due to the use of the fluorescent cholesterol analogue DHE. The alternating variation of AAPH-induced sterol oxidation with sterol content also appeared in multicomponent unilamellar vesicles containing bovine brain sphingomyelins (bbSPM), POPC, and DHE. The present work and our previous study on cholesterol oxidase-induced sterol oxidation [Wang et al. (2004) *Biochemistry 43,* 2159−2166] suggest that sterol oxidation in general, either by reactive oxygen species or by enzymes, may be regulated by the extent of sterol superlattice in the membrane and thus regulated by the membrane sterol content in a fine-tuning manner.

Cholesterol is a major component of mammalian cell membranes and lipoprotein particles. Cholesterol can be oxidized to 25-hydroxycholesterol, 7-ketocholesterol, cholest-4-en-3-one, and other oxysterols by enzymes of the cytochrome P450 family, reactive oxygen species (ROS)[1] and light exposure. Oxysterols (oxidation products of cholesterol) influence cholesterol homeostasis and transport by delaying post-prandial clearance of chylomicron remnants (*1*), impairing macrophage cholesterol export (*2*), and suppressing both sterol regulatory element binding protein (SREBP) processing (*3*) and insulin-induced gene 1 (INSIG1) gene expression (*4*). In humans, oxysterols have been linked to the etiology of cardiovascular diseases, apoptosis, neurological disorders, and cancer formation (*5*−*9*).

On the other hand, cholesterol oxidation could be beneficial. Generally, the oxidation process drastically reduces the half-life of the sterol molecule and helps to direct it to leave the body. In addition, oxysterols possess characteristics that are favorable for a signaling molecule and are thought to play a role in signal transduction (*9*, *10*). Thus, it is important to know how sterol oxidation is regulated.

In this study, we shall focus on ROS-induced sterol oxidation in membranes. ROS (e.g., superoxide, hydroxyl, and peroxide radicals) are continuously being produced in the body by cellular respiration, immune system defenses, and other functions. For instance, cytochrome P-450 enzymes in the endoplasmic reticulum generate superoxide radicals during the hydroxylation reactions of xenobiotics. Phagocytic leukocytes generate superoxides to kill engulfed bacteria (*11*). ROS are also present in our environment and in the foods we ingest. Under normal circumstances, the body has sufficient protective mechanisms to scavenge ROS and prevent toxicity. However, aging and many diseases (e.g., cancer, atherosclerosis, and Alzheimer's) are linked to oxidative damage of membrane lipids from ROS as a result of an imbalance between radical-generating and -scavenging systems (*12*−*14*). Clearly, an understanding of mechanisms that regulate the rate and extent of ROS-induced sterol oxidation would have far-reaching implications.

In the oxidation of membrane cholesterol, the physical properties of membranes should play an important role. Cholesterol lateral organization is one of the most important membrane physical properties, but how it affects cholesterol

† This work was supported by American Heart Association (0255082N) and in part by the American Chemical Society Petroleum Research Fund (PRF#38205-AC7). M.O. and S.-I.Y. were supported by Temple University fellowship. M.O. is currently a recipient of an American Heart Association postdoctoral fellowship (0425617U).

* Corresponding author. Phone: (215) 707-4182. Fax: (215) 707-7536. E-mail: pchong02@temple.edu.

[1] Abbreviations: AAPH, 2,2′-azobis (2-amidinopropane) dihydrochloride; bbSPM, bovine brain sphingomyelins; C_a, sterol mole fractions for maximal ROS-induced sterol oxidation; C_r, theoretically predicted critical sterol mole fractions for maximal superlattice formation; DHE, dehydroergosterol; MLV, multilamellar vesicles; LUV, large unilamellar vesicles; POPC, 1-palmitoyl-2-oleoyl-L-α-phosphatidylcholine; ROS, reactive oxygen species.

10.1021/bi047710s CCC: $30.25
Published on Web 01/22/2005

oxidation has not yet been studied to any great extent. This situation arises from two obstacles: the lack of a detailed molecular description for cholesterol lateral organization and the lack of reliable and sensitive methods to monitor cholesterol oxidation without perturbing cholesterol lateral organization. The first obstacle has been mitigated by the recent advent of sterol superlattice (refs *15*−*24*, reviewed in ref *25*) and sterol−phospholipid complex formation (*26*, *27*) models plus the concept of the umbrella effect (*28*, *29*); these have improved our understanding of sterol lateral organization at the molecular level.

In this study, we have developed a new fluorescence assay to deal with the second obstacle. This assay is able to monitor the relationship between sterol oxidation and sterol lateral organization. This novel assay uses dehydroergosterol (DHE) as both a membrane probe and a membrane component. The structure and physical properties of DHE are very similar to those of cholesterol (*30*, *31*). DHE also behaves similarly to cholesterol and ergosterol in terms of sterol superlattice formation (*18*, *19*). In the present study, sterol oxidation was induced by a free radical generator, AAPH (2,2′-azobis-(2-amidinopropane)dihydrochloride). Using this new assay, we found evidence that the rate of AAPH-induced sterol oxidation is affected by the extent of sterol superlattice in unilamellar vesicles composed of 1-palmitoyl-2-oleoyl-L-α-phosphatidylcholine (POPC) and DHE (or DHE/cholesterol) as well as in multicomponent unilamellar vesicles containing bovine brain sphingomyelins (bbSPM), POPC, and DHE.

MATERIALS AND METHODS

Materials. DHE was obtained from Sigma (St. Louis, MO). The concentration of the DHE stock solution was calculated by absorbance in dioxane at 326 nm, using an extinction coefficient equal to 10 600 M^{-1} cm^{-1}. POPC, bbSPM, and cholesterol were purchased from Avanti Polar Lipids (Alabaster, AL). The concentrations of phospholipids in POPC and sphingomyelins stock solutions and in LUVs were determined by the method of Bartlett (*32*). The prooxidant AAPH was obtained from Aldrich (Milwaukee, WI).

Vesicle Preparation and Characterization. Calculated amounts of phospholipids and DHE were pipetted into tubes and dried under N_2 until there was no visible solvent; lipids were then dried overnight under vacuum. Next, lipids were reconstituted with 5.0 mL of 0.02% NaN_3, 0.1 mM EDTA, 50 mM Tris-HCl buffer (pH 7.0) at 37 °C, then flushed with N_2, and vortexed for 2 min at 37 °C to form multilamellar vesicles (MLVs). The MLVs were cooled to 4 °C for 30 min and then incubated at 37 °C for 30 min. This cooling−heating cycle was repeated three times to ensure an even distribution of lipids within each monolayer of the vesicles. After being exposed to three cycles of heat/cold to allow for thorough mixing, vesicles were left for 4 days at room temperature to come to thermal equilibrium. LUVs were then prepared from MLVs by extrusion (Lipex Biomembranes Inc., Vancouver, BC, Canada). The MLVs were extruded at 37 °C 10 times through two stacked 200 nm Nucleopore polycarbonate filters (Costar) under nitrogen gas pressure to form homogeneous LUVs. To avoid auto-oxidation of cholesterol, the LUV samples were then stored under N_2 at room temperature for ≥7 days prior to sterol oxidation measurements. During this time, phosphorus concentration was measured again to determine new phospholipid concentration after loss by extrusion (*24*).

Scheme 1: Production of Peroxy Radicals from Thermal Decomposition of AAPH

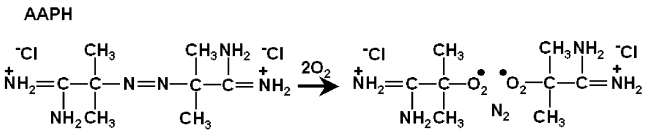

A typical LUV sample set spanned a predicted critical sterol mole fraction for maximal superlattice formation. Every sample within the set contained the same absolute amount of total sterol (DHE or DHE plus cholesterol) but varied only in the sterol mole percent. This was accomplished by varying the number of moles of phospholipids per tube, while leaving the number of moles of sterols constant. Typically, the sterol mole percent was increased by ∼0.3 mol % for each sample. Our previous study (*24*) shows that the sterol mole percents in vesicles before and after extrusion differ little (≤0.2 mol %). Thus, for convenience, the sterol mole percents in MLVs were used to assess the relationship between sterol content and sterol oxidation in LUVs.

Vesicle size was measured by photon correlation spectroscopy using the Malvern Zetasizer HS-1000 spectrometer (Malvern Worcs, UK; light source: 10 mW He−Ne laser at 633 nm). Size was determined before and immediately after extrusion, as well as after the 7−10 day incubation period. Vesicle size was also measured before and after some fluorescence assays. It was found that there was no significant change in vesicle size due to addition of AAPH. The possible presence of sterol microcrystals in the sample was checked by Rayleigh scattering using an SLM 8000C fluorometer (Urbana, IL) with the excitation set at 500 nm (0.5 nm band-pass) and emission at 505 nm (8 nm band-pass) (*33*).

Fluorescence Assay of Sterol Oxidation Induced by AAPH. Calculated amounts of DHE-containing LUVs and Tris-HCl buffer were added to cuvette for a total volume of 1.6 mL. LUVs were then incubated under a gentle magnetic stirring for 15 min at 37 °C in the sample compartment of the fluorometer. The sample temperature was achieved using a circulating bath. After incubation, time trace monitoring was begun. Excitation wavelength was 325 nm with a band-pass of 0.5 nm. The emission was observed at 396 nm through a monochromator with a band-pass of 8 nm. To initiate sterol oxidation, 30 μL of 300 mM freshly prepared AAPH was added. AAPH is a water-soluble free radical generator that undergoes thermal decomposition to yield N_2 plus two alkyl radicals, which then react with oxygen to form two peroxy radicals (*34*, *35*) (Scheme 1). AAPH-induced DHE oxidation was also measured by absorption at 326 nm using a Perkin-Elmer lambda-6 spectrophotometer (Shelton, CT).

RESULTS AND DISCUSSION

Figure 1 illustrates that AAPH-induced sterol oxidation can be monitored by DHE fluorescence. Before the addition of AAPH, the DHE fluorescence intensity (F_{obs}) is invariant with time. Upon addition of AAPH, there is an immediate sharp drop in DHE fluorescence intensity, followed by a steady decrease in fluorescence intensity over time (Figure 1). The sharp drop in F_{obs} is due to resonance energy transfer

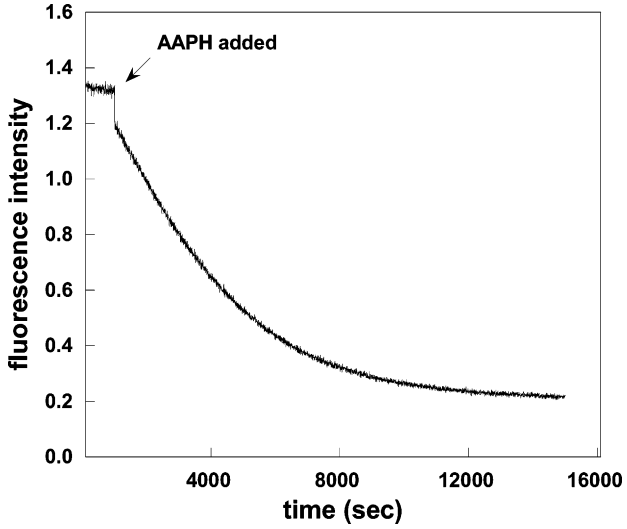

FIGURE 1: Profile of a typical assay showing DHE fluorescence intensity (F_{obs}) decay upon addition of AAPH to DHE (21.1 mol %)/POPC LUVs. F_{obs} was monitored at 395 nm. Temperature = 37 °C.

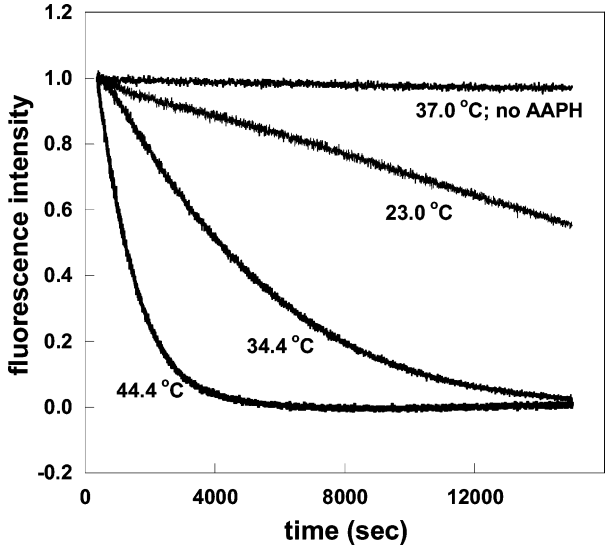

FIGURE 2: Temperature dependence of AAPH-induced DHE fluorescence intensity decay. POPC/DHE (21.2 mol %) LUVs were incubated at 44.4 °C (D), 34.4 °C (C), and 23.0 °C (B), respectively. Pro-oxidant, AAPH, was added at 60 s, and the rate of intensity decay was monitored. Rate of decay due to photobleaching alone (i.e., in the absence of AAPH) was measured at 37 °C (A).

between DHE and AAPH (acceptor) since the absorption spectrum of AAPH (nonfluorescent) overlaps with the emission spectrum of DHE. When less AAPH was added, the intensity drop due to energy transfer was reduced (data not shown). Energy transfer does not affect the calculations of initial rate or rate constant of sterol oxidation because energy transfer occurs much faster than sterol oxidation. The steady decrease in F_{obs} (immediately following the sharp intensity drop due to energy transfer) reflects sterol oxidation. DHE contains a conjugated triene in the tetracyclic steroid ring. Upon oxidation, the degree of double-bond conjugation would be reduced, leading to a decrease in fluorescence intensity. The fluorescence intensity measured at a long time after addition of AAPH is designated as F_∞, which is typically 10% of the initial intensity. The existence of a nonzero F_∞ value is probably due to either unreacted DHE in an inaccessible area or due to the production of a weakly fluorescent product.

The half-life of AAPH in neutral aqueous solutions is ~175 h at 37 °C, and the rate of AAPH-induced radical formation is constant for the first few hours (*34*, *35*). Therefore, the AAPH-induced steady decrease in DHE fluorescence intensity seen in Figure 1 cannot be attributed to variations in the rate of free radical formation. Further, in the absence of AAPH, the fluorescence intensity of DHE in POPC LUV drops only 0.5% over 5 h under our experimental conditions (trace A in Figure 2). Thus, the AAPH-induced steady decrease of DHE fluorescence intensity over time seen in Figure 1 is not due to photobleaching. Traces B−D in Figure 2 show the temperature dependence of AAPH-induced sterol oxidation. As expected, initial rate of sterol oxidation increased with increasing temperature.

To analyze data and determine if the AAPH-induced sterol oxidation is first or second order, a logarithmic plot and a reciprocal plot of the data were generated. For a first-order reaction, the concentration of reactant decreases exponentially with time ([reactant]/[reactant]$_{t=0}$ = exp(−kt)); thus, a plot of ln[reactant] versus time should be linear. For a second-order reaction, 1/[reactant] = kt + 1/[reactant]$_{t=0}$; consequently, a plot of 1/[reactant] versus time is linear. In our study, the reactant concentration (i.e., [DHE]) is proportional to the fluorescence intensity of DHE (F_{obs}). We found that a plot of ln F_{obs} versus time was linear, whereas a plot of 1/F_{obs} versus time was nonlinear (data not shown), indicating a first-order reaction scheme overall. Using a curve-fitting program (Kaleidagraph; v. 3.52; Synergy Software, Reading, PA), we can also demonstrate that the steady decrease of DHE fluorescence intensity induced by AAPH is best described by first-order kinetics (Figure 3A), as opposed to second-order kinetics (Figure 3B). The mechanism of the AAPH-induced sterol oxidation reaction in DHE-containing membrane bilayers is not clearly understood because the elementary steps involved in this complex reaction have not been elucidated. Nevertheless, the overall first-order kinetics could be attributed to the possibility that the rate-limiting elementary step of this complex reaction is first order (*36*).

DHE oxidation by AAPH was also monitored by absorbance at 326 nm. The absorbance decreases upon addition of AAPH (data not shown). The time course of the absorbance decay is also best fit to the equation for a first-order reaction, as is the case of AAPH-induced DHE fluorescence intensity decay (Figure 3A). This result suggests that the AAPH-induced decay of DHE fluorescence intensity is due to the AAPH-induced change of the DHE ground-state structure rather than the change in excited state. In other words, the absorption data support the idea that the AAPH-induced DHE fluorescence intensity decay (Figures 1 and 2) is due to free radical induced sterol oxidation.

Since first-order kinetics best describes the DHE fluorescence intensity decay upon addition of AAPH, we have used this same kinetic equation to fit (via Kaleidagraph, v.3.52) the DHE oxidation data to determine the apparent reaction rate constant, k. In DHE (23.4 mol %)/POPC LUVs, an addition of 30 μL of 300 mM AAPH at 37 °C yielded an apparent reaction rate constant $k = 3.78 \times 10^{-4} \pm 1.67 \times 10^{-5}$ s^{-1} (±SD) from six trials, showing a good reproducibility of the assay.

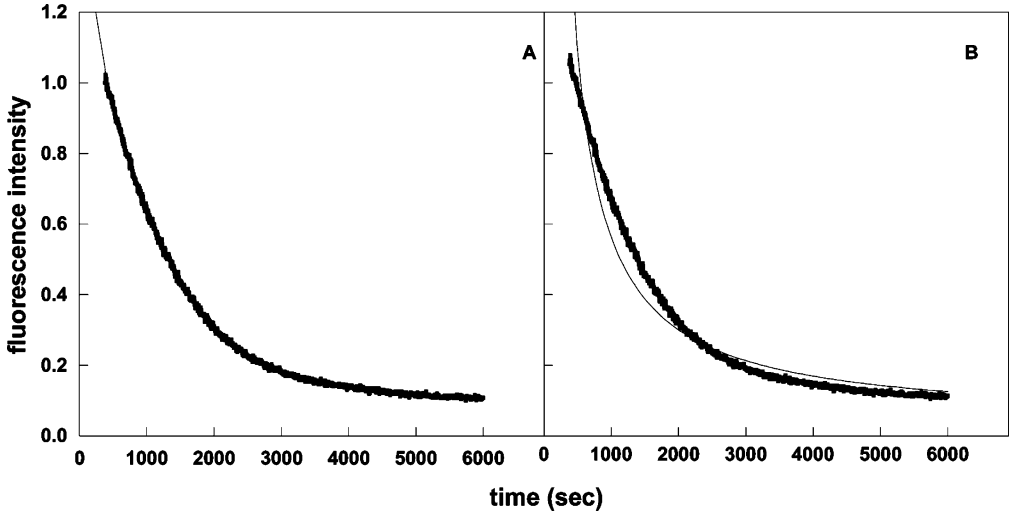

FIGURE 3: Data of the AAPH-induced DHE fluorescence decay in 21.2 mol % DHE/POPC LUVs measured at 37 °C are fitted by first-order (A) and second-order (B) kinetics. The fluorescence intensity (F_{obs}) at time zero (upon addition of AAPH) was normalized to unity. For first-order kinetics (A), the equation $[DHE]/[DHE]_0 = F/F_o = (F_{obs} - F_\infty)/F_o = \exp(-kt + b)$ was used, where b is a constant, and $[DHE]_o$ and F_o denote the DHE concentration and fluorescence intensity, respectively, at time zero, and a correlation coefficient $R = 0.999$ was obtained. For second-order kinetics (B), the equation $F_{obs} = 1/kt + F_\infty$ was used, and a correlation coefficient $R = 0.974$ was obtained. k is the apparent rate constant of the reaction, and F_∞ is the normalized DHE fluorescence intensity at a long time.

In addition to k, the initial rate, R_i, of the steady DHE intensity decrease can be determined from the kinetic trace. These two parameters (k and R_i) give a basis for comparison of results for samples within a sample set. Using the data shown in Figure 2 (traces B−D), we have determined both k and R_i of AAPH-induced sterol oxidation in DHE/POPC LUVs at three different temperatures. The k and R_i values exhibit a similar temperature dependence (data not shown) with an activation energy (calculated from an Arrhenius plot) of 28.6 ± 0.97 kcal/mol (±SD) determined from k and 29.3 ± 0.13 kcal/mol (±SD) from R_i, indicating that either k or R_i is a useful kinetic parameter for our comparison studies.

It is, however, important to emphasize that the initial rate R_i is preferred when addressing the relationship between sterol oxidation and sterol organization. Only the initial events can be meaningfully linked to cholesterol superlattice formation. After the reaction proceeds for a prolonged time, original lipid lateral organization may be perturbed by the random insertion of the reaction products (oxysterols). Oxysterols are known to have weaker interactions with membrane phospholipids than the parent sterols (*37*); this can also alter the original membrane lateral organization.

Figure 4 shows the effect of DHE mole fraction in POPC/DHE LUVs on the normalized initial rate (R_i) of AAPH-induced DHE fluorescence intensity decay at 37 °C. Despite that, in each set, the amounts of AAPH and DHE used were constant, the initial rate was not constant with sterol mole fraction. Instead, a biphasic change in initial rate appeared at 20.3, 22.2, 25.0, 32.3, and 40.0 mol % DHE. These mole fractions are either at or near the critical sterol mole fractions (20.0, 22.2, 25.0, 33.3, and 40.0 mol %) predicted for maximal superlattice formation (reviewed in ref *25)* in the concentration ranges examined (18.8−21.2, 21.5−23.4, 23.7−26.5, 28.6−34.5, and 38.5−42.4 mol % sterol). Within the experimental errors of sterol mole fractions (≤0.4 mol %, as calculated by error propagations of phospholipids and sterol concentration determinations, ref *19*), the observed critical mole fractions for maximum initial rate of oxidation

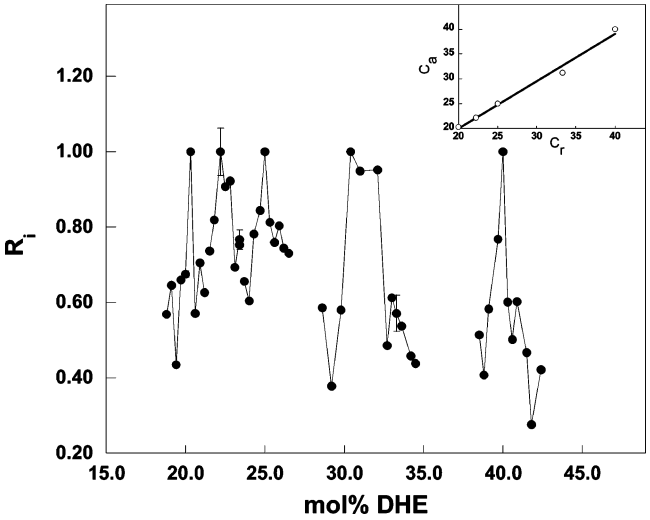

FIGURE 4: Plot of initial rate of DHE oxidation (R_i) vs DHE mole fraction in POPC/DHE LUVs over the entire sterol mole fraction range examined, with the peak rate in each separate set normalized to unity. The error bars are the typical standard deviations obtained from three independently prepared samples. Inset: the observed critical sterol mole fractions for maximum initial rate of oxidation (C_a) vs the predicted critical mole fractions for maximal sterol superlattice formation (C_r).

(C_a) (Figure 4) generally agree with the predicted critical mole fractions (C_r), giving a linear correlation coefficient (R) = 0.987 (inset in Figure 4).

The R_i peak position is reproducible, with a deviation of ≤0.4 mol %, similar to the fluctuation of the DHE intensity dip position determined previously in our laboratory from 16 independently prepared sample sets (*19*). But the shape of the initial rate peak may vary from experiment to experiment, which is reasonable, as the thermal history of each set of membrane preparation cannot be exactly identical. This phenomenon has been noticed and discussed in previous studies of lipid superlattices (*25*). An R_i peak (Figure 4) is judged to be genuine when the peak height is significantly larger than the standard deviations of the mean (vertical bars

in Figure 4) and when there is more than one data point located on either slope of the peak.

The results shown in Figure 4 are novel but explainable by the sterol superlattice model (*15*, *25*, *38*−*40*). The model proposes that areas of regular distribution of lipids (sterol superlattices) and areas of irregularly distributed lipids coexist in sterol-containing membranes, with the ratio of regular to irregular regions reaching a local maximum at critical sterol mole fractions (C_r) (e.g., 15.4, 20.0, 22.2, 25.0, 33.3, 40.0, and 50.0 mol % sterol). The model further proposes that sterol in the regular region is more accessible to the aqueous phase, due to tighter packing, than that in the irregular region. This property may arise from two possibilities. First, in the regular regions, sterol molecules are embedded less deeply than those in the irregular regions. Second, sterol in the regular regions is less shielded from water by the neighboring phospholipid polar headgroups than that in the irregular regions. In either case, at C_r, sterols should become more exposed to aqueous phase, where the bulk AAPH or soluble surface-acting enzymes reside. This explains well why sterol oxidation induced by the enzyme cholesterol oxidase (*24*) and by ROS (this study) is greater at C_r than at non-C_r. These two studies show that slight differences in the mole fraction of sterol could lead to large differences in the rate of enzymatic or free radical oxidation of sterol.

Although the biphasic change seen at or near critical mole fraction can be explained in terms of the sterol superlattice model, it is necessary to explore possible alternative explanations that might also produce this sort of result. If sterol molecules formed microcrystals at critical sterol mole fractions, there might be a sudden change in the rate of sterol oxidation at C_r. The maximum solubility of cholesterol in PC bilayers occurs at 66.7 mol % (*41*). When cholesterol mol % exceeds this maximum value, excess cholesterol leaves the bilayer in the form of monohydrate crystals, as revealed by X-ray diffraction. This solubility limit concentration is far beyond those examined in this study; thus, this alternative explanation is unlikely. To check experimentally for the possible sterol microcrystal formation in our membranes being examined, we have employed the method of Parker et al. (*33*). The method uses 90° light scattering to detect the presence of cholesterol monohydrate crystals in lipid bilayers by exploiting differences in size, structure, and refractive index. As cholesterol crystals are formed in the bilayer membrane and enter or leave the illumination beam in a cuvette (due to Brownian motion), large fluctuations in scattering intensity are introduced. A fluctuation parameter was defined as the standard deviation of the intensity fluctuation divided by the average intensity (σ/mean) (*33*). When cholesterol microcrystals were formed at 66.7 mol % cholesterol in PC bilayers, this parameter (σ/mean) underwent an abrupt increase (ref *33*; also see the open symbols in Figure 5B reproduced from ref *33*). The abrupt change in this parameter at 66.7 mol % cholesterol matches with the direct detection of microcrystals by X-ray diffraction at the same mole fraction. Thus, light scattering based on the parameter σ/mean is a convenient method for detecting cholesterol microcrystal formation in PC bilayers.

We have used this method to determine whether sterol crystals are formed in our POPC/DHE LUVs. Figure 5A shows the time dependence of the scattering intensity of LUVs composed of 24.7 mol % DHE in POPC. Fluctuation

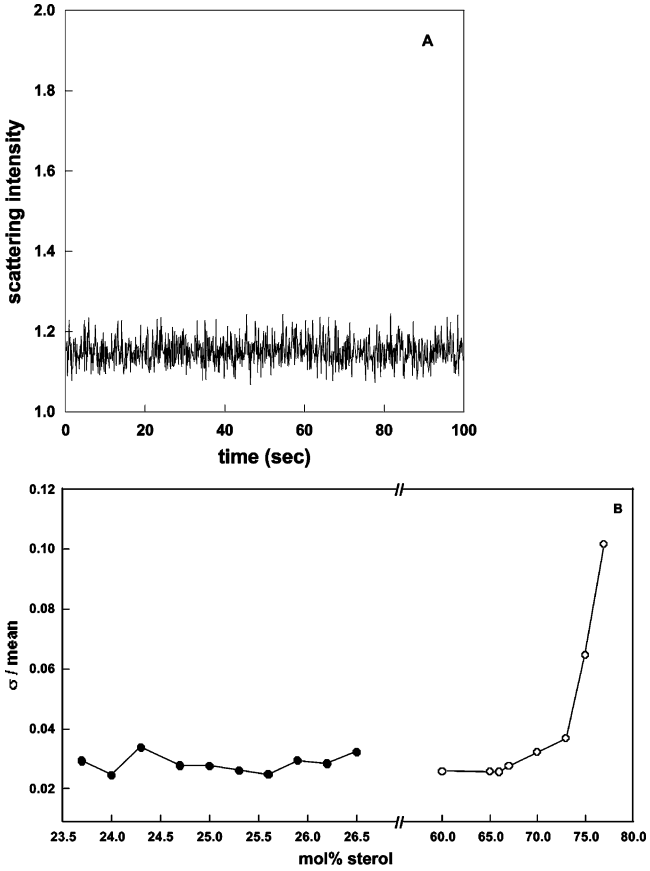

FIGURE 5: (A) Light scattering intensity vs time for DHE (24.7 mol %)/POPC LUVs. (B) Dark symbols: standard deviation (σ)/mean intensity of light scattering vs mol % DHE in DHE/POPC LUVs measured 37 °C. Open symbols: data taken from ref *33* for cholesterol in PC bilayers where sterol microcrystals are formed at 66.7 mol % cholesterol.

in scattering intensity is similar to that previously published for cholesterol-PC mixtures below the solubility limit and is much smaller than that seen in a sample with sterol mol % above the solubility limit (*33*). From the data shown in Figure 5A, a standard deviation divided by the intensity mean (σ/mean) can be obtained. The experiment was then repeated for different sterol mole fraction samples. The results are shown in Figure 5B (dark symbols). The σ/mean values in this concentration range (Figure 5B, dark symbols) remain low (∼0.03), characteristic of PC without sterol microcrystals (open circles below 66.7 mol % sterol in Figure 5B reproduced from ref *33*). The fluctuation parameter (σ/mean) should display a marked increase in the presence of sterol microcrystals (ref *33*; also the open symbols above 66.7 mol % sterol in Figure 5B).

To provide evidence that the alternating variation of initial rate of sterol oxidation is not due to some artifact of DHE fluorescence, three-component (DHE/cholesterol/POPC) LUVs were prepared, with DHE mol % fixed at 1 and 5 mol %. A distinct peak in initial rate of sterol oxidation is observable at 19.3−19.7 and 20.0−20.7 mol **%** total sterol in mixtures containing 1 and 5 mol % DHE, respectively (Figure 6). These peak positions are near the predicted critical mole fraction, 20.0 mol %, for the concentration range examined. The data (Figure 6) clearly show that it is the total sterol content, not the fluorescent proportion that causes the biphasic change in the rate of sterol oxidation. This result is

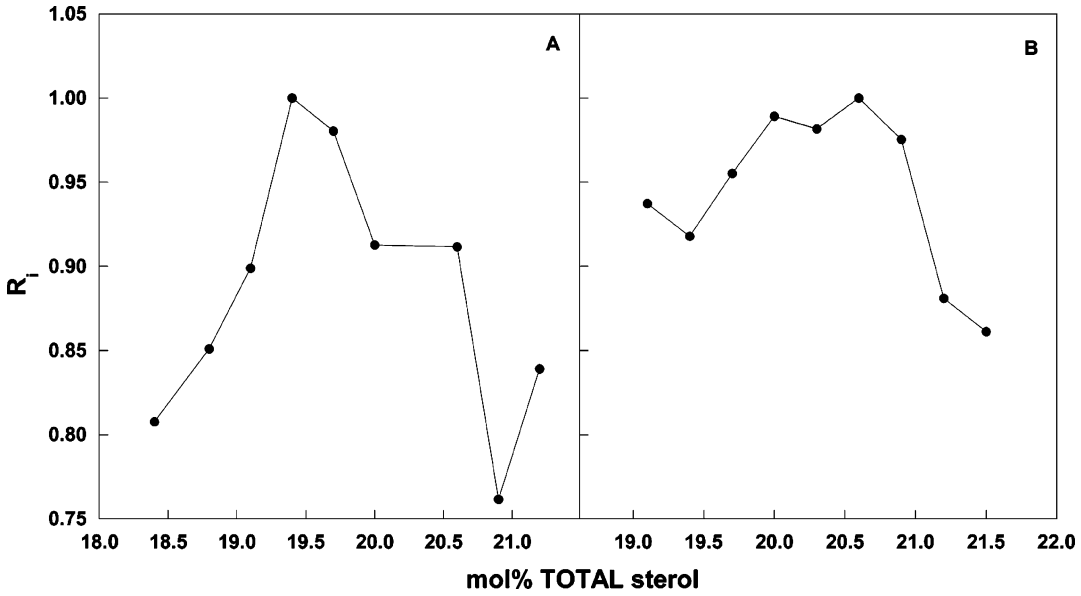

FIGURE 6: Normalized initial rate (R_i) of DHE oxidation vs mol % total sterol in three-component LUVs of DHE/cholesterol/POPC containing 1 mol % (A) and 5 mol % (B) DHE. Biphasic change in initial rate appeared near the predicted critical mol %. Plots were normalized by setting peak initial rate equal to unity. Mean vesicle size: 162 nm; assay performed at 37 °C. Total sterol = mol % DHE + mol % cholesterol.

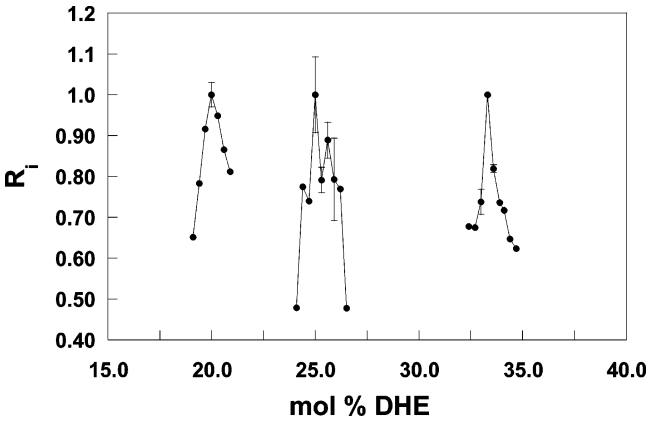

FIGURE 7: Effect of DHE mole fraction on the initial rate (R_i) of AAPH-induced DHE oxidation in POPC/bbSPM/DHE LUVs (140 nm in diameter) in three concentration regions: 19.1−20.9 mol % DHE (measured at 37 °C), 24.1−26.5 mol % DHE (measured at 24 °C), and 32.4−34.7 mol % (measured at 37 °C). The peak rate in each separate set is normalized to unity. The error bars are the typical standard deviations obtained from three independently prepared samples.

consistent with previous studies using mixtures of DHE, another sterol and phospholipids (*19*). In DHE/cholesterol/DMPC, DHE/ergosterol/DMPC, and DHE/cholesterol/DPPC multilamellar vesicles (MLVs), both DHE fluorescence intensity and DHE lifetime measurements exhibited dips whenever total sterol was at or near the critical mole fraction (DHE mole fraction was fixed at 5 mol %) (*19*).

Figure 7 shows the effect of sterol content on the initial rate of AAPH-induced DHE oxidation in multicomponent LUVs composed of DHE, POPC, and bovine brain sphingomyelins (bbSPM). The fatty acid content of bbSPM is 18:0 (57.99%), 24:1 (14.71%), 22:0 (9.16%), 24:0 (7.04%), 20:0 (6.08%), 16:0 (2.36%), and others (2.66%) (Avanti Polar Lipids catalog). In this multi-component membrane system, a biphasic change in initial rate of sterol oxidation was observed at 20.0, 25.0, and 33.3 mol % in the three concentration regions examined (19.1−20.9, 24.1−26.5, and 32.4−34.7 mol % DHE) (Figure 7). These three peak mole fractions are in excellent agreement with the critical sterol mole fractions theoretically predicted (i.e., 20.0, 25.0, and 33.3 mol %) in these three concentration ranges examined. The observation of biphasic changes in sterol oxidation at C_r in multicomponent liposomes argues for the possible existence of sterol superlattices in lipid bilayer regions of biological membranes.

For DHE (20.0 mol)/POPC/bbSPMs LUVs, the initial rate of AAPH-induced sterol oxidation was examined at three temperatures: 30, 37, and 42 °C (data not shown). The Arrhenius plot of the data yields an activation energy of sterol oxidation to be 17.4 ± 0.20 kcal/mol (±SD). This value was lower than 28.6 kcal/mol found in 18.4 mol % DHE/POPC two component LUVs mentioned earlier. It is likely that the packing becomes less efficient as more components are added to the system, so that sterol molecules are more easily oxidized overall when compared to those in a two-component system.

All the results presented in this study are in support of the sterol superlattice model (*15*, *25*, *38*). The model predicts that membrane properties should vary with sterol content in an alternating manner, showing local minima or maxima at C_r. Our previous model membrane studies have shown that the membrane partitioning of the antifungal drug nystatin (*20*), the hydrolytic activity and binding of snake venom phospholipase A2 (*21*, *42*), and the sterol oxidation activity of soil bacteria cholesterol oxidase (*24*) all vary with membrane sterol content in an alternating manner, showing a biphasic change at several C_r's. The present study shows that this membrane behavior holds true for the ROS-induced sterol oxidation.

The type of experimental work described here can be extended to cells. It is possible to incorporate DHE into living cells (*43*) and then monitor the ROS-induced DHE oxidation by examining the time course of the DHE fluorescence intensity decay. The physical principle revealed in our present model membrane study is likely to hold true in cell

membranes. This point is supported by the multicomponent results shown in Figure 7 and by previous studies of Na^+/K^+-ATPase. When reconstituted into lipid vesicles, the Na^+/K^+-ATPase activity showed a biphasic change with cholesterol content (*44*). Interestingly, the Na^+/K^+-ATPase activities of pig and bovine kidney basolateral membranes also decreased when the cholesterol content was above or below the native concentration (*45*, *46*), although it is not clear whether the biphasic change of the Na^+/K^+-ATPase activity occurs at the C_r and whether the biphasic activity change occurs at only one of the C_rs or can occur at multiple C_rs.

The present work on AAPH-induced sterol oxidation and the previous study on cholesterol oxidase-induced sterol oxidation (*24*) suggest that sterol oxidation in general, either by reactive oxygen species (ROS) or by enzymes, may be regulated by the extent of sterol superlattice in the membrane and thus by the membrane sterol content in a fine-tuning manner according to the principles of sterol superlattice formation. This fine-tuning is reasonable because oxysterols can be both beneficial and detrimental, as mentioned in the introductory paragraphs. A fine balance is needed to take advantage of the beneficial effect but prevent oxidative damage. This illustrates again the functional importance of minute changes in membrane sterol content (*20*, *21*, *24*).

It is possible that cells are able to adjust the level of membrane cholesterol in response to oxidative stress. Failure to do so may result in excess oxysterol production; this is known to have cytotoxic effects on many cell types, including neurons, smooth muscle cells, and vascular cells (*7*, *14*), and to be associated with the etiology of many diseases, such as Alzheimer's Disease, diabetes, atherosclerosis, and cancer (*5*−*9*). For example, excess oxysterols can induce apoptosis in vascular cells, a major event in the pathophysiology of atherosclerosis (*47*). An extensive accumulation of oxysterols in the subendothelial space may lead to inflammation and subsequent formation of atherogenic plaques (*48*). These adverse effects of oxysterols could be alleviated by therapeutically adjusting the cell's membrane cholesterol content according to the principle of sterol superlattice formation, as implicated by the present work and the previous study on cholesterol oxidase-induced sterol oxidation (*24*).

ACKNOWLEDGMENT

The authors are grateful to Prof. Juyang Huang for use of his data from ref 33 in Figure 5B.

REFERENCES

1. Vine, D. F., Croft, K. D., Beilin, L. J., and Mamo, J. C. (2002) Effect of dietary cholesterol oxidation products on the plasma clearance of chylomicrons in the rat, *Lipids 37*, 455−462.
2. Van Reyk, D. M., and Jessup, W. (1999) The macrophage in atherosclerosis: modulation of cell function by sterols, *J. Leukocyte Biol. 66*, 557−561.
3. Gimpl, G., Burger, K., and Farenholz, F. (2002) A closer look at the cholesterol sensor, *Trends Biochem. Sci. 27*, 596−599.
4. Janowski, B. A. (2002) The hypocholesterolemic agent LY295427 up-regulates INSIG-1, identifying the INSIG-1 protein as a mediator of cholesterol homeostasis through SREBP, *Proc. Natl. Acad. Sci. U.S.A. 99*, 12675−12680.
5. Saucier, S. E., Kandutsch, A. A., Taylor, F. R., Spencer, T. A., Phirwa, S., and Gayen, A. K. (1985) Identification of regulatory oxysterols, 24(*S*),25-epoxycholesterol and 25-hydroxycholesterol, in cultured fibroblasts, *J. Biol. Chem. 260*, 14571−14579.
6. Steinberg, D. (1991) Antioxidants and atherosclerosis. A current assessment, *Circulation 84*, 1420−1425.
7. Peng, S., Hu, B., and Morin, R. J. (1992) Effects of cholesterol oxides on atherogenesis, in *Biological Effects of Cholesterol Oxides* (Peng, S., and Morin, R. J., Eds.) Ch. 9, CRC Press, Boca Raton, FL.
8. Jackson, S. M., Ericsson, J., and Edwards, P. A. (1997) Signaling molecules derived from the cholesterol biosynthetic pathway, in *Subcellular Biochemistry*, Vol. 28 (Bittman, R., Ed.) Plenum Press, New York.
9. Bjorkhem, I. (2002) Do oxysterols control cholesterol homeostasis? *J. Clin. Invest. 110*, 725−730.
10. Lange, Y., Ye, J., and Strebel, F. (1995). Movement of 25-hydroxycholesterol from the plasma membrane to the rough endoplasmic reticulum in cultured hepatoma cells, *J. Lipid Res. 36* (5), 1092−1097.
11. Dahlgren, C., and Karlsson, A. (1999) Respiratory burst in human neutrophils, *J. Immunol. Methods 232*, 3−14.
12. Ames, B. N., Shigenaga, M. K., Hagen, T. M. (1993) Oxidants, antioxidants, and the degenerative diseases of aging, *Proc. Natl. Acad. Sci. U.S.A. 90*, 7915−7922.
13. Moslen, M. T. (1994) in *Free Radicals in Diagnostic Medicine* (D. Armstrong, Ed.) Plenum Press, New York.
14. Panini S. R., and Sinensky M. S. (2001) Mechanisms of oxysterol-induced apoptosis, *Curr. Opin. Lipidol. 12*, 529−533.
15. Chong, P. L.-G. (1994) Evidence for regular distribution of sterols in liquid crystalline phosphatidylcholine bilayers, *Proc. Natl. Acad. Sci. U.S.A. 91*, 10969−10073.
16. Virtanen, J. A., Ruonala, M., Vauhkonen, M., and Someharju, P. (1995) Lateral organization of liquid-crystalline cholesterol-dimyristoylphosphatidylcholine bilayers. Evidence for domains with hexagonal and centered rectangular cholesterol superlattices, *Biochemistry 34*, 11568−11581.
17. Parasassi, T., Giusti, A. M., Raimondi, M., and Gratton, E. (1995) Abrupt modifications of phospholipid bilayer properties at critical cholesterol concentrations, *Biophys. J. 68*, 1895−1902.
18. Chong, P. L.-G., Liu, F., Wang, M. M., Truong, K., Sugar, I. P., and Brown, R. E. (1996) Fluorescence evidence for cholesterol regular distribution in phosphatidylcholine and in sphingomyelin lipid bilayers, *J. Fluor. 6*, 221−230.
19. Liu, F., Sugar, I. P., and Chong, P. L.-G. (1997) Cholesterol and ergosterol superlattices in three-component lipid crystalline lipid bilayers as revealed by dehydroergosterol fluorescence, *Biophys. J. 72*, 2243−2254.
20. Wang, M. M., Sugar, I. P., and Chong, P. L.-G. (1998) Role of sterol superlattice in the partitioning of antifungal drug nystatin into lipid membranes, *Biochemistry 37*, 11797−11805.
21. Liu, F., and Chong, P. L.-G. (1999) Evidence for a regulatory role of cholesterol superlattices in the hydrolytic activity of secretory phospholipase A2 in lipid membranes, *Biochemistry 38*, 3867−3873.
22. Wang, M. M., Sugar, I. P., and Chong, P. L.-G. (2002) Effect of double bond position on dehydroergosterol fluorescence intensity dips in phosphatidylcholine bilayers with saturated *sn*-1 and monoenoic *sn*-2 acyl chains, *J. Phys. Chem. 106*, 6338−6345.
23. Cannon, B., Heath, G., Huang, J., Somerharju, P., Virtanen, J. A., and Cheng, K. H. (2003) Time-resolved fluorescence and Fourier transform infrared spectroscopic investigations of lateral packing defects and superlattice domains in compositionally uniform phosphatidylcholine bilayers, *Biophys. J. 84*, 3777−3791.
24. Wang, M. M., Olsher, M., Sugár, I. P., and Chong, P. L.-G. (2004) Cholesterol superlattice modulates the activity of cholesterol oxidase in lipid membranes, *Biochemistry 43*, 2159−2166.
25. Chong, P. L.-G., and Sugar, I. P. (2002) Fluorescence studies of lipid regular distribution in membranes, *Chem. Phys. Lipids 116*, 153−175.
26. Radhakrishnan, A., Anderson, T., and McConnell, H. M. (2000) Condensed complexes, rafts, and the chemical activity of cholesterol in membranes, *Proc. Natl. Acad. Sci. U.S.A. 97*, 12422−12427.
27. McConnell, H. M., and Vrljic, M. (2003) Liquid−liquid immiscibility in membranes, *Annu. Rev. Biophys. Biomol. Struct. 32*, 469−492.
28. Huang, J., and Feigenson, G. W. (1999) A microscopic interaction model of maximum solubility of cholesterol in lipid bilayers, *Biophys. J. 76*, 2142−2157.
29. Huang, J. (2002) Exploration of molecular interactions in cholesterol superlattices: Effect of multibody interactions, *Biophys. J. 83*, 1014−1025.

30. Schroeder, F. (1984) Fluorescent sterols: probe molecules of membrane structure and function, *Prog. Lipid Res. 23*, 97−113.
31. Chong, P. L.-G., and Thompson, T. E. (1986) Depolarization of dehydroergosterol in lipid bilayers, *Biochim. Biophys. Acta 863*, 53−62.
32. Bartlett, G. R. (1959) Phosphorus assay in column chromatography, *J. Biol. Chem. 234*, 466−468.
33. Parker, A., Miles, K., Cheng, K. H., and Huang, J. (2004) Lateral distribution of cholesterol in dioleoylphosphatidylcholine lipid bilayers: cholesterol−phospholipid interactions at high cholesterol limit, *Biophys. J. 86*, 1532−1544.
34. Niki, E. (1990) Free radical initiators as source of water- or lipid-soluble peroxyl radicals, *Methods Enzymol. 186*, 100−108.
35. Krasowska, A., Rosiak, D., Szkapiak, K., Oswiecimska, M., Witek, S., and Lukaszewicz, M. (2001) The antioxidant activity of BHT and new phenolic compounds PYA and PPA measured by chemiluminescence, *Cell. Mol. Biol. Lett. 6*, 71−81.
36. Laidler, K. J., and Meiser, J. H. (1999) in *Physical Chemistry*, 3rd ed., p 422, Houghton Mifflin Company, Boston, MA.
37. Moore, N. F., Patzer, E. J., Barenholz, Y., and Wagner, R. R. (1977) Effect of phospholipase C and cholesterol oxidase on membrane integrity, microviscosity, and infectivity of vesicular stomatitis virus, *Biochemistry 16*, 4708−4715.
38. Chong, P. L.-G., and Olsher, M. (2005) Fluorescence studies of the existence and functional importance of regular distributions in liposomal membranes, *Soft Mater.*, in press.
39. Sugar, I. P., Tang, D., and Chong, P. L.-G. (1994) Monte Carlo simulation of lateral distribution of molecules in a two-component lipid membrane. Effect of long-range repulsive interactions, *J. Phys. Chem. 98*, 7201−7210.
40. Tang, D., and Chong, P. L.-G. (1992) E/M dips: evidence for lipids regularly distributed into hexagonal super-lattices in pyrene-PC/DMPC binary mixtures at specific concentrations, *Biophys. J. 63*, 903−910.
41. Huang, J., Buboltz, J. T., and Feigenson, G. W. (1999) Maximum solubility of cholesterol in phosphatidylcholine and phosphatidylethanolamine bilayers, *Biochim. Biophys. Acta 1417*, 89−100.
42. Chong, P. L.-G. (1996) Membrane-Free volume variation with bulky lipid concentration by regular distribution: An important membrane property explored by pressure studies of phosphatidylcholine bilayers, in *High-Pressure Effects in Molecular Biophysics and Enzymology* (Markley, J. L., Northrop, D. B., and Royer, C. A., Eds.) pp 298−313, Oxford University Press, New York.
43. McIntosh, A. L., Gallegos, A. M., Atshaves, B. P., Storey, S. M., Kannoju, D., and Schroeder, F. (2003) Fluorescence and multiphoton imaging resolve unique structural forms of sterol in membranes of living cells, *J. Biol. Chem. 278*, 6384−6403.
44. Cornelius, F. (1995) Cholesterol modulation of molecular activity of reconstituted shark Na^+,K^+-ATPase, *Biochim. Biophys. Acta 1235*, 205−212.
45. Sotomayor, C. P., Aguilar, L. F., Cuevas, F. J., Helms, M. K., and Jameson, D. M. (2000) Modulation of pig kidney Na^+/K^+-ATPase activity by cholesterol: role of hydration, *Biochemistry 39*, 10928−10935.
46. Yeagle, P. L., Young, J., and Rice, D. (1988) Effects of cholesterol on (Na^+,K^+)-ATPase ATP hydrolyzing activity in bovine kidney, *Biochemistry 27*, 6449−6452.
47. Martinet, W., and Kockx, M. M. (2001) Apoptosis in atherosclerosis: focus on oxidized lipids and inflammation, *Curr. Opin. Lipidol. 12*, 535−541.
48. Hodis, H. N., Chauhan, A., Hashimoto, S., Crawford, D. W., and Sevanian, A. (1992) Probucol reduces plasma and aortic wall oxysterol levels in cholesterol fed rabbits independently of its plasma cholesterol lowering effect, *Atherosclerosis 96*, 125−134.

BI047710S